Quark spin and orbital angular momentum from proton generalized parton distributions

Adam Freese [1,2,*] and Ian C. Cloët[1,†]
[1]*Argonne National Laboratory, Lemont, Illinois 60439, USA*
[2]*Department of Physics, University of Washington, Seattle, Washington 98195-1560, USA*

(Received 27 January 2021; accepted 18 March 2021; published 14 April 2021)

We calculate the leading-twist helicity-dependent generalized parton distributions (GPDs) of the proton at finite skewness in the Nambu–Jona-Lasinio (NJL) model of quantum chromodynamics (QCD). From these (and previously calculated helicity-independent GPDs) we obtain the spin decomposition of the proton, including predictions for quark intrinsic spin and orbital angular momentum. The inclusion of multiple species of diquarks is found to have a significant effect on the flavor decomposition, and resolving the internal structure of these dynamical diquark correlations proves essential for the mechanical stability of the proton. At a scale of $Q^2 = 4$ GeV^2 we find that the up and down quarks carry an intrinsic spin and orbital angular momentum of $S_u = 0.534$, $S_d = -0.214$, $L_u = -0.189$, and $L_d = 0.210$, whereas the gluons have a total angular momentum of $J_g = 0.151$. The down quark is therefore found to carry almost no total angular momentum due to cancellations between spin and orbital contributions. Comparisons are made between these spin decomposition results and lattice QCD calculations.

DOI: 10.1103/PhysRevC.103.045204

I. INTRODUCTION

How the proton's spin is shared among its constituents is one of the most pressing open questions in hadron physics. Ever since the European Muon Collaboration found that the quarks' intrinsic spin falls far short of saturating the proton's total spin [1], various theoretical efforts have gone both into accounting for the remaining spin and into exploring the theoretical foundations for decomposing the proton's spin. For a review, see Ref. [2].

A prominent gauge-invariant decomposition of spin was proposed by Ji [3] using the flavor-separated gravitational form factors:

$$J_a = \tfrac{1}{2}[A_a(0) + B_a(0)], \tag{1}$$

where $a = q$ and g are the quark and gluon contributions. This allows the proton's spin to be decomposed into total contributions from each parton type. Because the total intrinsic spin of quarks is a gauge-invariant quantity, one may decompose J_q further into spin and orbital angular momentum, giving a proton spin decomposition:

$$\frac{1}{2} = \sum_q (S_q + L_q) + J_g. \tag{2}$$

This is called the Ji spin decomposition. A gauge-invariant decomposition of J_g into intrinsic and orbital angular momentum is not possible in this framework.

While alternative spin decompositions exist, the Ji spin decomposition has the virtue of being calculable from leading-twist generalized parton distributions (GPDs) [4–6]. In particular, polynomiality sum rules [7] relate the Mellin moments of GPDs to gravitational and axial form factors, which when evaluated at $t = 0$ give access to the total and spin angular momentum of partons. The GPDs are themselves of great contemporary interest because of their relationship to spatial light cone distributions [8], the proton's mass decomposition [9,10], and cross sections for hard exclusive reactions such as deeply virtual Compton scattering [5,11] that can be measured at facilities such as Jefferson Lab and the Electron Ion Collider.

It is therefore important to perform calculations of the proton's helicity-dependent and helicity-independent leading-twist GPDs within a single framework to make a unified set of predictions. It is vital that any model calculation must respect the symmetries and low-energy dynamical properties of quantum chromodynamics (QCD). Accordingly, we calculate the proton's helicity-dependent GPDs using the Nambu–Jona-Lasinio (NJL) model of QCD [12–14], an effective field theory that preserves all the global symmetries of QCD, reproduces dynamical chiral symmetry breaking, and can simulate aspects of confinement[1] through the use of proper time regularization [15–17]. Moreover, the NJL model has previously been used to calculate the helicity-independent proton GPDs [18], and because these calculations are symmetry-preserving, the baryon number, momentum, and angular momentum sum

*afreese@uw.edu
†icloet@anl.gov

[1]In particular, when using proper time regularization with an infrared cutoff, quark propagators contain no poles, and meson and baryon propagators do not develop an imaginary part at $p^2 > (2M)^2/(3M)^2$, preventing decay into the quark and antiquark constituents.

rules are automatically satisfied, as are constraints such as polynomiality and correct support properties.[2]

This paper is organized as follows. In Sec. II, we discuss the formalism used for calculating the helicity-dependent proton GPDs. In Sec. III, we present the results for the GPDs and for the spin decomposition they entail. Finally, in Sec. IV we present a summary and outlook.

II. FORMALISM FOR CALCULATING PROTON GPDs

The formalism for calculating the proton GPDs has been laid out already in Ref. [18]. However, we briefly review the formalism here, with additional elaborations relevant to the helicity-dependent case. The proton is considered as a bound state of three dressed quarks. The bound state amplitude is found by solving the Faddeev equation, which is dominated by configurations with two of the quarks in a diquark correlation [19]. In this work, we consider quark-diquark configurations specifically, in particular, configurations with isoscalar, Lorentz scalar, and isovector, axial vector diquarks. More information about the proton bound state amplitude can be found in Ref. [17].

The proton's helicity-dependent GPDs are defined from the axial bilocal lightcone correlator [4–6]:

$$A^q_{\lambda'\lambda} = \bar{u}(p',\lambda')\Big[\not{n}\gamma_5 \widetilde{H}^q(x,\xi,t) + \frac{\gamma_5(n\Delta)}{2M_N}\widetilde{E}^q(x,\xi,t)\Big]u(p,\lambda), \tag{3}$$

where $P = \frac{1}{2}(p'+p)$, $\Delta = p'-p$, $\xi = -2(\Delta n)/(Pn)$, $t = \Delta^2$, and n is a lightlike vector defining the light front. The GPDs are Lorentz-invariant functions of the three explicitly written Lorentz-invariant arguments and are also dependent on a renormalization scale μ not notated above. In the NJL model calculation, we take $\mu = M = 400$ MeV [17,20,21].

The axial correlator itself is calculated by evaluating Feynman diagrams, with the bilocal operator defining the GPDs inserted into either a quark within a diquark or into the accompanying quark; both scenarios are depicted diagrammatically in Fig. 1. To be more specific, we obtain analytic expressions for the GPDs by first taking arbitrary Mellin moments of the relevant Feynman diagrams and then analytically perform an inverse Mellin transform. By having analytic expressions for the Mellin moments in an intermediate step, we are able to explicitly verify that polynomiality is satisfied within the calculation. For the diquark propagators we implement the widely used pole approximation [22–30].[3] Self-consistency

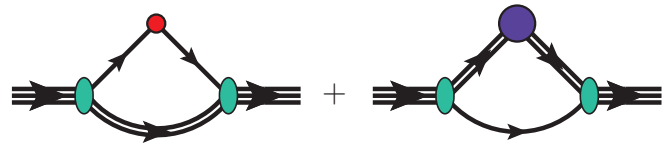

FIG. 1. Diagrams contributing to the leading-twist proton GPDs. On the left is the quark diagram and on the right is the diquark diagram. The single line is the dressed quark propagator, the double line is the diquark propagator, the shaded oval is the Faddeev vertex, and the shaded circles represent the dressed quark and diquark GPDs.

then demands that on-shell forms for the diquark GPDs be used [33], even though they are in general off-shell. These approximations mean that the inner structures of the diquarks are folded into the proton through a convolution relation, which takes the form [18]

$$H_X(x,\xi,t) = \int \frac{dy}{|y|} h_{Y/X}(y,\xi,t)\, H_Y\Big(\frac{x}{y},\frac{\xi}{y},t\Big), \tag{4}$$

where a hadron (proton) X contains a composite hadron (diquark) Y, and where $h_{Y/X}$ signifies "body GPDs" that encode the distribution of Y within X. The isospin weights for the quark and diquark diagrams, for each quark flavor, are given in Eqs. (102) and (103) of Ref. [17].

A. Helicity-dependent diquark GPDs

We proceed to consider the helicity-dependent GPDs of diquarks. We first remark that scalar diquarks do not have helicity-dependent GPDs, because the lack of total angular momentum does not provide a quantization axis. Thus we need consider just axial vector diquarks and transition GPDs between the two diquark species.

The axial vector diquark has four helicity-dependent GPDs. We parametrize the on-shell correlator in the following way:

$$\begin{aligned} A^{q,\mu\nu}_a = {} & \frac{(n\Delta)}{\Delta^2}\frac{i\epsilon_{\Delta\mu\nu P}}{(Pn)}\widetilde{H}^q_{1a}(x,\xi,t) \\ & - \frac{i\epsilon_{n\Delta P\mu}\Delta^\nu - i\epsilon_{n\Delta P\nu}\Delta^\mu + i(P\Delta)\epsilon_{n\mu\nu\Delta}}{\Delta^2(Pn)} \\ & \times\Big[-\widetilde{H}^q_{1a}(x,\xi,t) + \frac{\Delta^2}{M_a^2}\widetilde{H}^q_{2a}(x,\xi,t)\Big] \\ & - \frac{i\epsilon_{n\Delta P\mu}\Delta^\nu + i\epsilon_{n\Delta P\nu}\Delta^\mu}{M_a^2(Pn)}\widetilde{H}^q_{3a}(x,\xi,t) \\ & + \frac{i\epsilon_{n\Delta P\mu}n^\nu + i\epsilon_{n\Delta P\nu}n^\mu}{2(Pn)^2}\widetilde{H}^q_{4a}(x,\xi,t), \end{aligned} \tag{5}$$

where M_a is the axial vector diquark mass and we use the notation $\epsilon_{\Delta\mu\nu P} = \epsilon_{\alpha\mu\nu\beta}\Delta^\alpha P^\beta$ (i.e., a four-vector in the Levi-Civita subscripts signifies contraction with that four-vector).

[2]Note that parity-time symmetry and Poincaré invariance are sufficient to entail polynomiality, and that these symmetries alone are the premises used to prove that QCD satisfies polynomiality. Approximations that break these symmetries will result in violations of polynomiality, but no symmetry-breaking approximations are used in this work.

[3]Because calculations using the full diquark propagator have not been done, the accuracy of this approximation is hard to quantify. The suitability of this approximation is attested to by the results of Refs. [22–30]. The Dyson-Schwinger calculations of Refs. [31,32] are additionally suggestive, in that the baryon masses and electromagnetic form factors calculated therein show good agreement between a full three-body calculation and a quark-diquark approximation that uses the pole approximation for the diquark propagator.

When contracted with polarization vectors ε_μ and ε'^*_ν, this is equivalent to the standard form given in Ref. [34], owing to a Schouten identity and the fact that the polarization vectors are orthogonal to the diquark momenta. We choose the form in Eq. (5) in part because Δ has no virtuality dependence, thus being preferred over P for having a free Lorentz index, and in part because it prevents the appearance of unphysical poles in the axial form factors. (See the Appendix for more details on the elimination of these unphysical poles.)

Scalar-to-axial-vector and axial-vector-to-scalar (sa and as) transition GPDs must be considered. The bilocal axial correlator for scalar-to-axial transitions is

$$A^{q,\nu}_{\rm sa} = \frac{n^\nu M_{\rm as}}{(Pn)}\,\widetilde{H}_{{\rm sa},1}(x,\xi,t) + \frac{(n\Delta)\Delta^\nu}{(Pn)M_{\rm as}}\,\widetilde{H}_{{\rm sa},2}(x,\xi,t), \quad (6)$$

where $M_{\rm as} = M_s + M_a$ and M_s is the scalar diquark mass. There is an analogous expression for the axial-vector-to-scalar transition case. These GPDs have the property of being neither T-even nor T-odd. However, they remain related by time-reversal symmetry in a vital respect:

$$\widetilde{H}_{{\rm sa},i}(x,\xi,t) = -\widetilde{H}_{{\rm as},i}(x,-\xi,t). \quad (7)$$

Crucially, the proton body GPDs accompanying these diquark GPDs in the convolution formula, Eq. (4), exhibit this same property, which ensures that any T-odd contributions to the proton GPDs resulting from the diquark transition diagrams cancel out—a necessity, because proton GPDs are strictly T-even.

B. Dressed quark GPDs

The dressed quarks in the NJL model are quasiparticles arising from an amalgamation of nearly massless current quarks. Because GPDs are defined using bilocal operators of current quark fields, the dressed quarks have nontrivial GPDs that must be calculated within the NJL model and folded into hadrons via Eq. (4). As discussed in Ref. [18], the leading-twist dressed quark GPDs can be obtained by solving an inhomogeneous Bethe-Salpeter equation. For the helicity-dependent GPDs, one has $\not{n}\gamma_5\delta(n[xP-k])$ as a driving term.

We find the isoscalar and isovector helicity-dependent dressed quark GPDs to be as follows:[4]

$$\widetilde{H}_{I=0,1}(x,\xi,t) = \delta(1-x), \quad (8a)$$

$$\widetilde{E}_{I=0,1}(x,\xi,t) = \frac{N_c}{2\pi^2}\frac{1}{|\xi|}\frac{G_{\eta,\pi}M^2}{1+2G_{\eta,\pi}\Pi_{PP}(t)} \times\Gamma\left(0,\alpha/\Lambda^2_{\rm UV},\alpha/\Lambda^2_{\rm IR}\right)\Theta(|\xi|-|x|), \quad (8b)$$

where $\Gamma(s,a,b) = \int_a^b dt\, t^{s-1}\,e^{-t}$ is the generalized incomplete gamma function and $\alpha = M^2 - \frac{1}{4}(1-x^2/\xi^2)t$. We remark that the support region for the dressing functions [i.e., for the contributions to the GPDs other than $\delta(1-x)$] is entirely constrained to the Efremov-Radyushkin-Brodsky-Lepage (ERBL) region and thus that the PDF in particular is undressed. It is also worth noting that the GPD $\widetilde{E}_I(x,\xi,t)$ contains a pion pole or an η-meson pole, depending on the isospin.

[4]These results are without π-a_1 mixing for consistency with Ref. [17], from which we lift the model parameters.

III. RESULTS

With the formalism above, we proceed to present results for the helicity-dependent GPDs of the proton, as well as for the proton spin decomposition. Specifically, the model parameters from Ref. [17] are used. However, in addition, we also consider a model variant with only scalar diquarks. For this, the scalar diquark parameter G_s is found by solving proton's Faddeev equation with the proton mass fixed to its physical value. In the scalar-only model, we find $G_s = 9.98$ GeV^{-2} and $M_s = 576$ MeV.

A. Helicity-dependent proton GPDs

Helicity-dependent GPDs are presented for zero and finite skewness ($\xi = 0.5$) at the model scale $Q^2 = M^2$ in Fig. 2. Because the helicity-dependent GPD $\widetilde{E}^q(x,\xi,t)$ becomes large near $t = 0$ due to the presence of a pion pole, it is scaled by a factor of $\tau = -t/(4M_N^2)$. We see that for $\xi = 0$ our GPD results have no support for $-1 < x < 0$ because, at the model scale, we have not included antiquarks in the model calculation. However, at finite skewness an ERBL region ($-\xi < x < \xi$) develops and our GPDs are nonzero in the range $-\xi < x < 1$, even in this valence quark picture at the model scale. These results clearly show that GPDs at finite skewness can display features radically different from those at $\xi = 0$.

A visually significant aspect of the $\widetilde{E}^q(x,\xi,t)$ results in Fig. 2 is the jump discontinuities at $x = \pm\xi$. This occurs in effective theories with a four-fermion interaction vertex [35–37] and can be seen in the dressed quark GPD of Eq. (8b). On the surface this is an apparent problem for QCD factorization, which requires GPDs to be continuous across the Dokshitzer-Gribov-Lipatov-Altarelli-Parisi (DGLAP)-ERBL boundary. However, numerical studies suggest that these jump discontinuities are removed by GPD evolution, rendering the model calculations compatible with QCD factorization above the model scale and allowing Compton form factors to be rigorously calculated.

In Fig. 3, we present the same helicity-dependent proton GPDs as in Fig. 2, but evolved to a scale of $Q^2 = 4$ GeV^2 using leading-order kernels [5,11,38]. We find that the QCD evolution has a dramatic impact on $\widetilde{E}^q(x,\xi,t)$, which is now also continuous across the DGLAP-ERBL boundary.

In both Figs. 2 and 3 the range $0 \leqslant -t \leqslant 2$ GeV^2 was used to give a broad perspective on the functional form of the GPDs. It is worth noting that physical processes sensitive to the GPDs, such as deeply virtual Compton scattering, are accompanied by the kinematic constraint $-t < Q^2$. However, as formally defined via Eq. (3), the GPDs can be evaluated at any t. We present the large $-t$ behavior of the NJL model GPDs to ascertain their suitability for empirical predictions in this kinematic regime. In the presented figures, a slow $-t$ falloff can be observed. This behavior is known to be characteristic of contact interactions [39].

With both the helicity-dependent proton GPDs above and the previously calculated helicity-independent GPDs [18] in

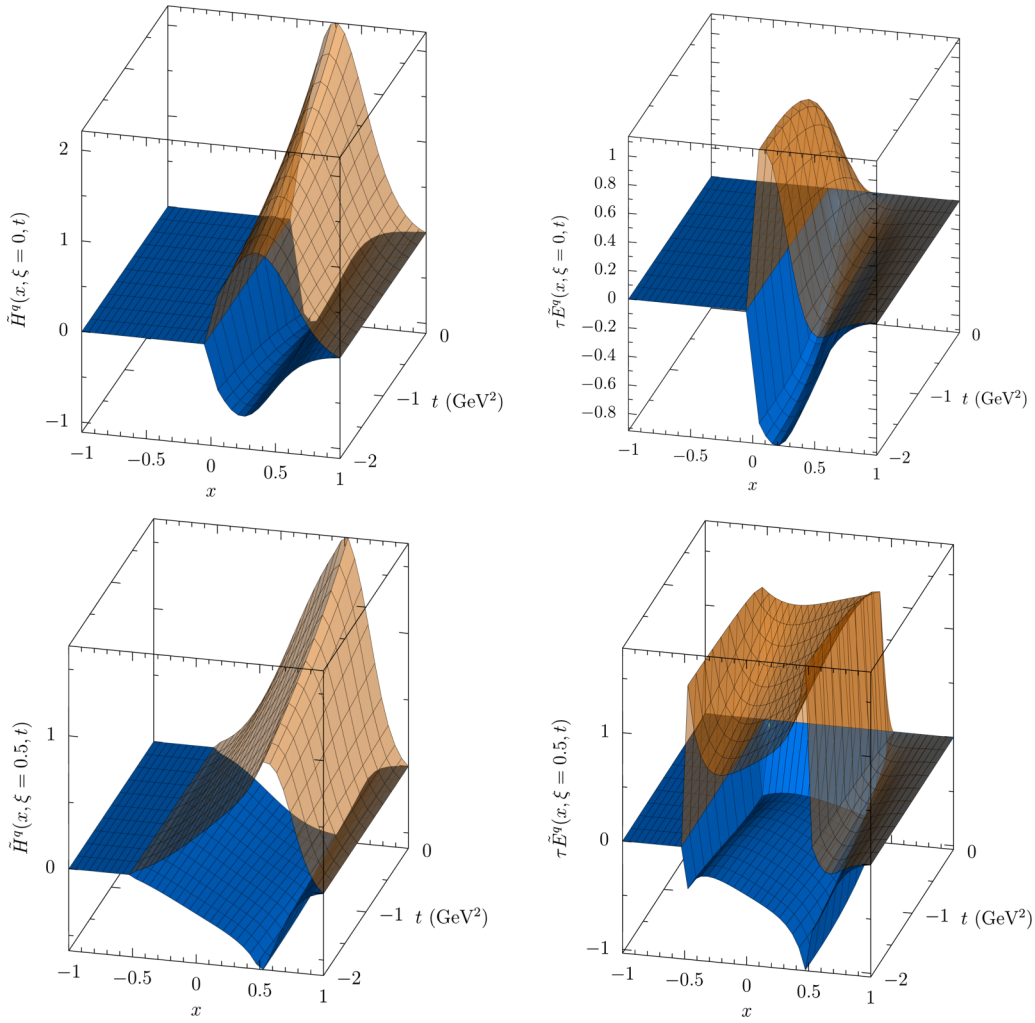

FIG. 2. The helicity-dependent proton GPDs at the model scale of $Q^2 = 0.16$ GeV^2, where the GPD $\widetilde{E}^q(x,\xi,t)$ has been scaled by a factor of $\tau = -t/(4M_N^2)$. The top row is for $\xi = 0$ and the bottom row has $\xi = 0.5$. The transparent (orange) surface is up quarks and the opaque (blue) surface is down quarks.

hand, we proceed to consider various static properties of the proton, with a special focus on its spin decomposition.

B. Static properties of the proton

Various static properties of the proton can be obtained from Mellin moments of the GPDs at $t = 0$. Several of these, such as the electric charge, the magnetic moment, the axial charge, and the quark spin S_q can be obtained from form factors and have been studied elsewhere (see Ref. [17] for electromagnetic properties). Others, such as the total angular momentum J, the anomalous gravitomagnetic moment $B(0)$, and the D-term $C(0)$ are new opportunities afforded through GPDs. The gravitational form factors $A(t)$, $B(t)$, and $C(t)$ can be obtained from the helicity-independent GPDs through

$$\sum_{a=q,g}\int_{-1}^{1} dx x H^a(x,\xi,t) = A(t) + \xi^2 C(t), \tag{9}$$

$$\sum_{a=q,g}\int_{-1}^{1} dx x E^a(x,\xi,t) = B(t) - \xi^2 C(t), \tag{10}$$

and the total angular momentum can then be obtained through the Ji sum rule in Eq. (1). Moreover, by not summing over parton flavors, one can obtain a flavor decomposition of these quantities, although such a breakdown will be renormalization scheme and scale dependent (unlike the sum, which is scheme and scale independent).

The quark spin can be obtained from the helicity-dependent GPDs:

$$S_q = \frac{1}{2}\int_{-1}^{1} dx \widetilde{H}^q(x,\xi,t=0), \tag{11}$$

and the quark orbital angular momentum can then be obtained through $L_q = J_q - S_q$. The isovector axial vector charge g_A is related to the up and down intrinsic spin via the Bjorken sum rule: $g_A = 2(S_u - S_d)$.

We present the results for various static quantities of the proton, along with a diagram-by-diagram breakdown, in Table I. In particular, these quantities are calculated with both scalar and axial vector diquarks present in the proton. The first two columns of results provide contributions to the

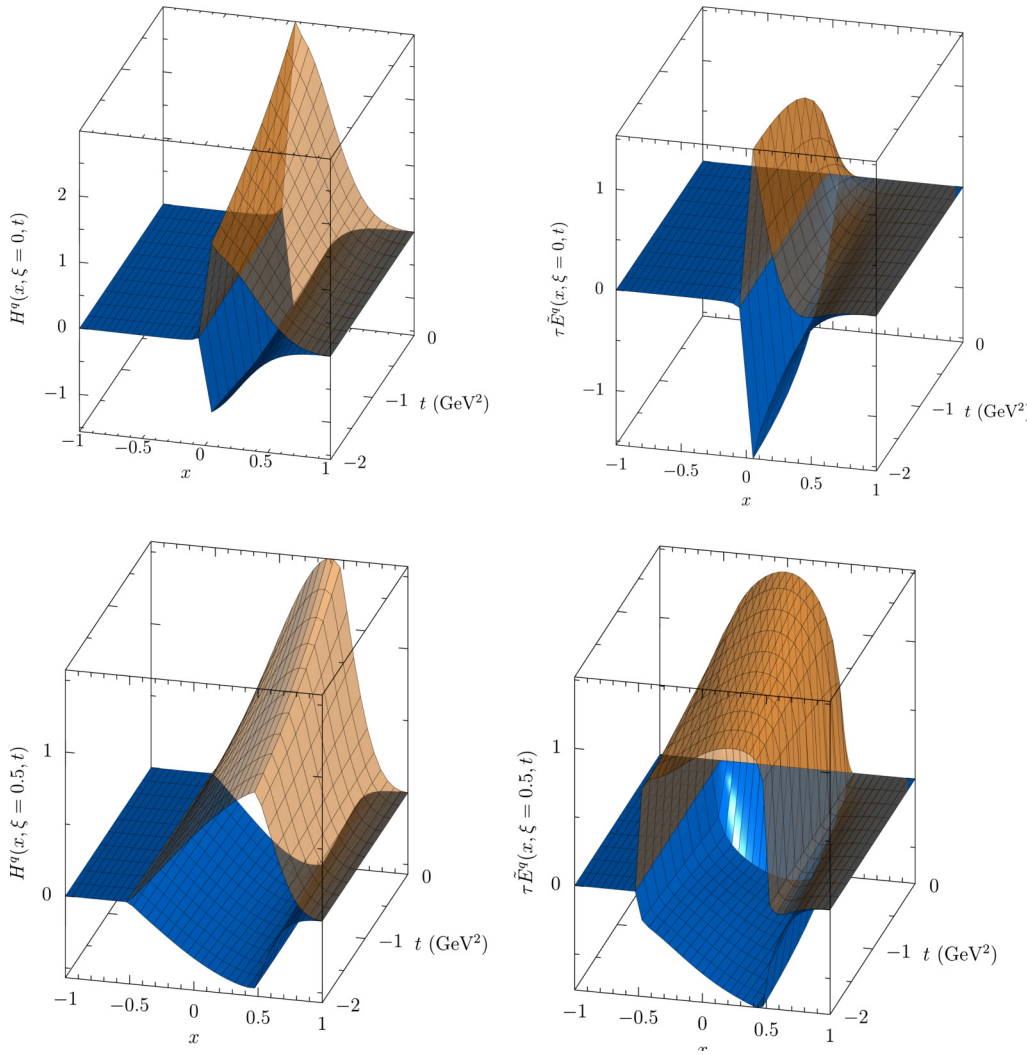

FIG. 3. The helicity-dependent proton GPDs at the scale of $Q^2 = 4.0$ GeV^2, where the GPD $\widetilde{E}^q(x,\xi,t)$ has been scaled by a factor of $\tau = -t/(4M_N^2)$. The top row is for $\xi = 0$ and the bottom row has $\xi = 0.5$. The transparent (orange) surface is up quarks and the opaque (blue) surface is down quarks.

proton's flavor-separated anomalous magnetic moment, which are included to provide a comparison with other results and because they would vanish in the absence of orbital angular momentum in the proton. The next two columns provide quark momentum factors in the proton, and we find that scalar diquark configurations carry about twice the light-cone momentum as the axial vector configurations. In addition, up quarks carry about two-thirds and down quarks about one-third of the total light-cone momentum, as naively expected.

For the flavor-separated quantities in Table I we first remark that not only does the total $B(0)$ vanish (as expected by angular momentum conservation) but also the total contribution from each diquark configuration vanishes. However, this is not the case for $B_u(0)$ or $B_d(0)$ separately. This is an

TABLE I. Decomposition of static properties of the proton by the various diagrammatic contributions, where the full scalar + axial diquark model is used. The quantities are given at the model scale of $Q^2 = 0.16$ GeV^2 and the diquark in the parentheses is the spectator.

Diagram	κ_u	κ_d	$A_u(0)$	$A_d(0)$	$B_u(0)$	$B_d(0)$	$C_u(0)$	$C_d(0)$	$S_{\rm tot}$	$L_{\rm tot}$	$J_{\rm tot}$	g_A
Quark (scalar)	1.134	0	0.248	0	0.306	0	0.020	0	0.287	−0.100	0.277	0.574
Scalar diquark	−0.546	−0.546	0.220	0.220	−0.153	−0.153	−0.516	−0.516	0	0.068	0.068	0
Quark (axial)	−0.150	−0.300	0.034	0.067	−0.060	−0.120	0.039	0.048	−0.066	0.026	−0.040	0.044
Axial diquark	0.785	0.157	0.176	0.035	0.150	0.030	−0.155	−0.031	0.137	0.058	0.195	0.182
Transition diquark	0.346	−0.346	0	0	0.108	−0.108	0.014	−0.014	0	0	0	0.751
Sum	1.569	−1.045	0.678	0.322	0.351	−0.351	−0.598	−0.483	0.358	0.142	0.500	1.551

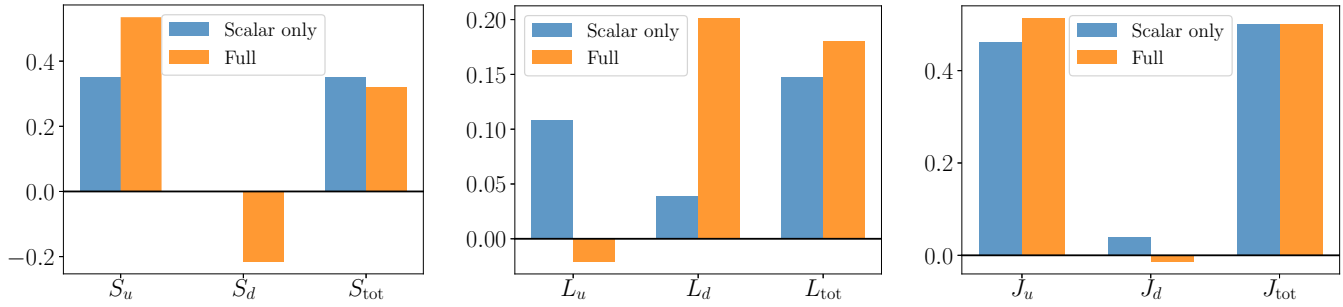

FIG. 4. Spin decomposition at the model scale. The scalar-diquark-only model variant is contrasted with the full model containing both scalar and axial vector diquarks.

observation similar to that found in Ref. [40], where each state in a Fock space expansion has $B(0) = 0$ and has the same formal cause: the diquark configuration (or the Fock state) has the same quantum numbers as the proton and is thus a $J = \frac{1}{2}$ eigenstate. Thus we can say $\langle J \rangle = \frac{1}{2}\langle x \rangle = \frac{1}{2}A(0)$ for each configuration (or Fock state) individually, entailing $B(0) = 0$.

We next remark on the $C(0)$ contributions of the various diagrams. The negativity condition [41], which states that $C(0) < 0$ is necessary for mechanical stability, is satisfied by both diquark configurations. In both cases, $C(0)$ is positive for the quark diagram and negative for the diquark diagram. This illustrates the necessity of resolving the dynamical diquark degrees of freedom to obtain a mechanically stable proton.

For the total intrinsic spin contribution $S_{\rm tot} = S_u + S_d$ we find that scalar diquark configurations dominate, even though the scalar diquark itself has no intrinsic spin. For $L_{\rm tot}$ and $J_{\rm tot}$ the situation is more subtle because of cancellations between different contributions. However, we note that diquark transition diagrams cannot contribute to conserved quantum numbers, because the scalar and axial vector diquark configurations are effectively orthogonal states. Moreover, the transition diagrams cannot contribute to any isoscalar quantities such as S, L, or $C(0)$ because the transition itself is isovector (namely, from an isovector to an isoscalar diquark, or vice versa). On the other hand, they can make a potentially large contribution to isovector quantities such as $S_u - S_d$. In fact, the transition diagram is responsible for nearly half of our calculated value for g_A. In this case, one can see that g_A is an overestimate compared to the experimental value of $g_A = 1.2732(23)$ [42]. This discrepancy can be alleviated by the inclusion of meson cloud effects, as done in Ref. [17] for the simpler calculations of proton electromagnetic form factors.

C. Proton spin decomposition

The leading-twist proton GPDs allow us to obtain the Ji decomposition of proton spin. In particular, the quark total angular momentum J_q can be broken up into S_q and L_q, and the total gluon angular momentum J_g can be obtained at an evolved scale from the perturbatively generated gluon GPDs. Because the Ji decomposition does not allow J_g to be broken into spin and orbital components, we use $S_{\rm tot}$ and $L_{\rm tot}$ to signify the total *quark* spin and orbital angular momentum.

In Fig. 4, we compare the proton spin decomposition at the model scale for both variants of our NJL model, that is, one where the proton has only scalar diquark correlations and the full model that also includes axial vector diquarks. Remarkably, the total angular momentum carried by each quark flavor, as well as the total quark spin and total quark orbital angular momentum change very little when axial vector diquarks are introduced. This may be attributed to the static approximation being used for the quark-diquark interaction kernel, where orbital angular momentum is generated by relativistic effects, in particular, by the presence of a p-wave component in the quark wave function [44]. Because the relativistic effects are about equally strong in both variants of the model, $L_{\rm tot}$ and $S_{\rm tot}$ are about equal.

In the scalar-only model, $S_d = 0$ because the down quark is present only in the diquark, which does not allow a spin quantization axis to be identified. Nonrelativistically, one would have $L_d = J_d = 0$ as well, but the remaining quark in the proton carrying orbital angular momentum—since it can exist in a p-wave state—implies that the diquark, and thus the down quark, can carry orbital angular momentum as well. The diagram breakdown for the full model in Table II indeed shows that L_d and J_d are nonzero because of the scalar diquark diagram.

The flavor breakdown of J, L, and S changes significantly when axial vector diquarks are present, for two reasons. The first—but more minor—reason is that the flavor breakdown within axial diquark configurations differs from that of the scalar diquark case. The effects of this are minimal, however, and due entirely to relativistic effects. Nonrelativistically

TABLE II. Flavor decomposition of the total, spin, and orbital angular momenta, where the results include contributions from both scalar and axial vector diquarks. Results are at the model scale of $Q^2 = 0.16\ \text{GeV}^2$ and the diquark in the parentheses is the spectator.

Diagram	J_u	J_d	S_u	S_d	L_u	L_d
Quark (scalar)	0.277	0	0.287	0	−0.010	0
Scalar diquark	0.034	0.034	0	0	0.034	0.034
Quark (axial)	−0.013	−0.026	−0.022	−0.044	0.009	0.018
Axial diquark	0.163	0.033	0.114	0.023	0.049	0.010
Transition diquark	0.054	−0.054	0.188	−0.188	−0.134	0.134
Sum	0.514	−0.014	0.567	−0.209	−0.053	0.195

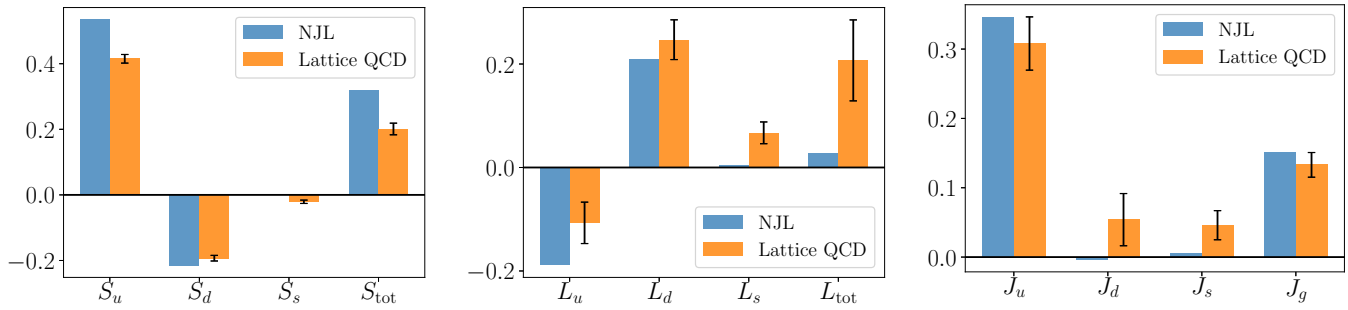

FIG. 5. Comparison of NJL model spin decomposition to the lattice QCD results of Ref. [43] at $Q^2 = 4$ GeV^2. The NJL results contain contributions from both scalar and axial vector diquarks.

(and within the static approximation), there is no orbital angular momentum, and the axial diquark configuration has a spin wave function: $|J_p^z = +\frac{1}{2}\rangle = \sqrt{\frac{2}{3}}|J_{\rm dq}^z = +1; J_q^z = -\frac{1}{2}\rangle - \sqrt{\frac{1}{3}}|J_{\rm dq}^z = 0; J_q^z = +\frac{1}{2}\rangle$, which when combined with the appropriate isospin recombination coefficients gives $J_d = S_d = 0$. Indeed, even within the proper NJL model calculation, we find the contributions to J_d and S_d from the axial diquark diagrams are 0.006 and -0.021, respectively.

The most significant contributions to the change in flavor breakdown come from transition diagrams. Although J is a conserved quantity, individual flavor contributions are not. Moreover, individual flavor contributions are not isoscalar, and in fact $J_u - J_d$, etc., are isovector, meaning the transition diagram has the potential to make significant changes to these differences. In fact, as can be seen in Table II, S_d and L_d are dominated by the transition diagram, although this diagram makes a small contribution to J_d.

Overall, J_d comes out very close to zero in the scalar + axial model. This can be seen as arising from cancellations. On one hand, S_d and L_d end up being nearly equal and opposite after contributions from all the diagrams have been summed. On the other hand, in Table I, one sees that $A_d(0)$ and $B_d(0)$ are nearly equal and opposite after summing the diagrams.

Besides intermodel comparisons, it is worth comparing our flavor-separated proton spin decomposition to the best available estimates for the true proton spin decomposition. Although experimental extractions for linear combinations of J_u and J_d exist from JLab [45] and HERMES [46,47], these extractions are model dependent and may not be instructive. On the other hand, there exists a lattice QCD computation of the proton spin decomposition at physical pion mass [43].

In Fig. 5, we compare our results (with both diquark species present) to the lattice results of Ref. [43] at a scale of $Q^2 = 4$ GeV^2. One can observe mixed agreement with the lattice results. First, it is worth remarking that the broad qualitative agreement on the sign and magnitude of J_u, J_d, L_u, L_d, S_u, and S_d is remarkable considering the simplicity and minimalism of the NJL model. This is suggestive that the spin decomposition of the proton is governed to a large extent by three effects: its diquark content, relativistic effects that can generate L, and QCD evolution (which connects the model scale to the empirical scale). Further intricacies (such as a meson cloud) could be somewhat large but seem to be second-order effects. Solving the Faddeev equation beyond the static approximation will also have an impact; however, because the spin decomposition is defined through $t = 0$ moments, the effects of exchange diagrams are expected to be small.

The agreement for J_g is surprising, because in our calculation this is generated purely by QCD evolution, and is therefore suggestive of a small intrinsic gluon angular momentum. Our calculations also tend to overestimate S_q for the light quarks, which could be rectified by the inclusion of a pion and kaon cloud, which would also generate the missing intrinsic S_s contributions. Because J_q agrees reasonably well with lattice, corrections that decrease S_q would at the same time need to increase L_q, which is natural in the meson cloud picture because of their p-wave couplings to the quarks or the nucleon.

IV. SUMMARY AND OUTLOOK

In this work, we calculated the helicity-dependent and helicity-independent leading-twist proton GPDs in a confining version of the NJL model. A quark-diquark approximation was used for the proton, and two variants of the model were considered: (i) a model with only isoscalar, Lorentz scalar diquarks, and (ii) a model also containing isovector, axial vector diquarks. In both model variants, a flavor-separated spin decomposition was performed for the proton, and the presence of both diquark species was found to contribute significantly to the flavor-separated spin decomposition, but little to $S_{\rm tot}$ and $L_{\rm tot}$. In particular, transition diagrams between the diquark species—which can affect only isoscalar quantities, such as $S_u - S_d$—were responsible for most of the difference between the models' spin decompositions.

The model variant with both diquarks present was found to have mixed agreement with lattice results for the proton's spin decomposition. The discrepancies are due primarily to the NJL model's overestimates of spin and underestimates of orbital angular momentum, along with the lack of strangeness content. The former of these discrepancies can be resolved by the inclusion of a pion cloud, and the latter can be resolved with the inclusion of a kaon cloud. These improvements warrant future work on the subject.

ACKNOWLEDGMENTS

This work was supported by the U.S. Department of Energy, Office of Science, Office of Nuclear Physics, Contract

No. DE-AC02-06CH11357, and an LDRD initiative at Argonne National Laboratory under Project No. 2020-0020. A.F. was additionally supported by U.S. Department of Energy Grant No. DE-FG02-97ER-41014.

APPENDIX: LONGITUDINAL-TRANSVERSE SEPARATION FOR AXIAL OPERATORS

The nonlocal operator defining the helicity-dependent GPDs, as well as the local axial current, is defined using matrix elements of the operator $\bar{q}(x)\gamma_\mu\gamma_5 q(y)$, with the space-time points x and y determined by the application in question. This operator notoriously does not correspond to a conserved current. However, it is possible to break the operator into a "transverse" piece that is conserved and a "longitudinal" piece that is not. The breakdown is most clear in momentum space, where we define

$$(\gamma_\mu\gamma_5)_\perp = \left(\gamma_\mu - \frac{\Delta_\mu \not{\Delta}}{\Delta^2}\right)\gamma_5, \quad (\gamma_\mu\gamma_5)_\parallel = \frac{\Delta_\mu \not{\Delta}}{\Delta^2}\gamma_5, \tag{A1}$$

with Δ being the momentum transfer to the target. That $(\gamma_\mu\gamma_5)_\perp$ is transverse to Δ makes $\bar{q}(x)(\gamma_\mu\gamma_5)_\perp q(x)$ a conserved local current.

Notably, the dynamics of $\bar{q}(x)(\gamma_\mu\gamma_5)_\perp q(y)$ and $\bar{q}(x)(\gamma_\mu\gamma_5)_\parallel q(y)$ completely decouple. This means that the Bethe-Salpeter equations for the local currents $\bar{q}(0)(\gamma_\mu\gamma_5)_\perp q(0)$ and $\bar{q}(0)(\gamma_\mu\gamma_5)_\parallel q(0)$ decouple from each other and also that the BSEs for the leading-twist nonlocal correlators

$$A^q_{\perp,\parallel} = \frac{1}{2}\int\frac{dz}{2\pi}e^{ix(Pn)\kappa}\langle p'\lambda'|\bar{q}\left(-\frac{nz}{2}\right)(\not{n}\gamma_5)_{\perp,\parallel}\left[-\frac{nz}{2},\frac{nz}{2}\right]q\left(\frac{nz}{2}\right)|p\lambda\rangle, \tag{A2}$$

decouple from each other.

The Lorentz decompositions of the transverse and longitudinal components of the helicity-dependent correlator can be written, for a spin-half particle, as

$$A^q_{\perp,\lambda'\lambda} = \bar{u}(p',\lambda')(\not{n}\gamma_5)_\perp u(p,\lambda)\,\widetilde{H}(x,\xi,t), \tag{A3}$$

$$A^q_{\parallel,\lambda'\lambda} = \bar{u}(p',\lambda')(\not{n}\gamma_5)_\parallel u(p,\lambda)\,[\widetilde{H}(x,\xi,t) - \tau\widetilde{E}(x,\xi,t)] \equiv \bar{u}(p',\lambda')(\not{n}\gamma_5)_\parallel u(p,\lambda)\,\widetilde{E}_\parallel(x,\xi,t). \tag{A4}$$

Comparing to Eq. (8), we observe that the pion pole can contribute only to the longitudinal component of the correlator. This additionally means that the pion pole will not be present in $\widetilde{H}^q(x,\xi,t)$—nor $G_A(t)$—of the proton.

For an on-shell spin-one particle, the longitudinal-transverse separation can be written as

$$A^q_{\perp,\lambda'\lambda} = -i\left(\frac{\epsilon_{n\Delta P\rho}}{\Delta^2}\frac{\varepsilon^\rho(\varepsilon'^*\Delta) - \varepsilon'^{*\rho}(\varepsilon\Delta)}{(Pn)} + \frac{(P\Delta)}{\Delta^2}\frac{\epsilon_{n\varepsilon\varepsilon'^*\Delta}}{(Pn)}\right)\left[-\widetilde{H}^q_1 + \frac{\Delta^2}{M_a^2}\widetilde{H}^q_2\right] - \frac{i\epsilon_{n\Delta P\rho}}{M_a^2}\frac{\varepsilon^\rho(\varepsilon'^*\Delta) + \varepsilon'^{*\rho}(\varepsilon\Delta)}{(Pn)}\widetilde{H}^q_3$$
$$+ \frac{i\epsilon_{n\Delta P\rho}}{2(Pn)}\frac{\varepsilon^\rho(\varepsilon'^* n) + \varepsilon'^{*\rho}(\varepsilon n)}{(Pn)}\widetilde{H}^q_4, [0] \tag{A5a}$$

$$A^q_{\parallel,\lambda'\lambda} = \frac{(n\Delta)}{\Delta^2}\frac{i\epsilon^{\Delta\varepsilon\varepsilon'^*P}}{(Pn)}\widetilde{H}^q_1. \tag{A5b}$$

This breakdown agrees exactly with the standard breakdown in Ref. [34] for on-shell particles, through use of the Schouten identity result,

$$(n\Delta)\epsilon^{\Delta\varepsilon\varepsilon'^*P} = \Delta^2\epsilon^{n\varepsilon\varepsilon'^*P} - \epsilon^{n\Delta P\sigma}[\varepsilon_\sigma(\varepsilon'^*\Delta) - \varepsilon'^*_\sigma(\varepsilon\Delta)] - (\Delta P)\epsilon^{n\varepsilon\varepsilon'^*\Delta}, \tag{A6}$$

and the on-shell relation $(\Delta P) = 0$, as well as use of the identities $(\varepsilon\Delta) = 2(\varepsilon P)$ and $(\varepsilon'^*\Delta) = -2(\varepsilon^* P)$.

For an off-shell particle, $(\Delta P) \neq 0$ means the equivalence between the decompositions no longer holds. Crucially, the decompositions differ by a transverse structure that multiplies a longitudinal GPD. This means using the standard decomposition for an off-shell spin-one particle will introduce unphysical pion poles into transverse quantities, such as $G_A(t)$ of the proton. Therefore, the alternative decomposition suggested in Eq. (A5)—which indeed does not produce unphysical pion poles in the proton's axial form factor—is preferred for the off-shell spin-one correlator.

One last crucial aspect of Eq. (A5) worth remarking on is the explicit inclusion of a term proportional to $(P\Delta)$. For an on-shell spin-one particle, this term is zero and is not important. For an off-shell particle, however, it is necessary for the axial correlator $A^q_{\lambda'\lambda}$ to be analytic at $t = 0$. Neither the Lorentz structure multiplying $\widetilde{H}^q_1$ in Eq. (A5b) nor the structure multiplying $-\widetilde{H}^q_1 + \frac{t}{M_a^2}\widetilde{H}^q_2$ in Eq. (A5a) has a well-defined forward limit; if one writes $\Delta^\mu = \sqrt{-t}\,e^\mu$, with e^μ being an arbitrary spacelike unit vector, then the $t \to 0^-$ limit depends on e^μ, which is unphysical. However, by virtue of the Schouten identity, Eq. (A6), and the presence of the $(P\Delta)$ term in Eq. (A5a), the total axial correlator $A^q_{\parallel,\lambda'\lambda} + A^q_{\perp,\lambda'\lambda}$ does have a well-defined $t = 0$ limit, even when $(P\Delta) \neq 0$.

[1] J. Ashman *et al.* (European Muon Collaboration), Phys. Lett. B **206**, 364 (1988).
[2] E. Leader and C. Lorcé, Phys. Rep. **541**, 163 (2014).
[3] X.-D. Ji, Phys. Rev. Lett. **78**, 610 (1997).
[4] F. M. Dittes, D. Mueller, D. Robaschik, B. Geyer, and J. Horejsi, Phys. Lett. B **209**, 325 (1988).
[5] X.-D. Ji, Phys. Rev. D **55**, 7114 (1997).
[6] M. Diehl, Phys. Rep. **388**, 41 (2003).
[7] X.-D. Ji, J. Phys. G: Nucl. Part. Phys. **24**, 1181 (1998).
[8] M. Burkardt, Int. J. Mod. Phys. A **18**, 173 (2003).
[9] C. Lorcé, H. Moutarde, and A. P. Trawiński, Eur. Phys. J. C **79**, 89 (2019).
[10] Y. Hatta, A. Rajan, and K. Tanaka, J. High Energy Phys. 12 (2018) 008.
[11] A. V. Radyushkin, Phys. Rev. D **56**, 5524 (1997).
[12] U. Vogl and W. Weise, Prog. Part. Nucl. Phys. **27**, 195 (1991).
[13] S. P. Klevansky, Rev. Mod. Phys. **64**, 649 (1992).
[14] T. Hatsuda and T. Kunihiro, Phys. Rep. **247**, 221 (1994).
[15] D. Ebert, T. Feldmann, and H. Reinhardt, Phys. Lett. B **388**, 154 (1996).
[16] G. Hellstern, R. Alkofer, and H. Reinhardt, Nucl. Phys. A **625**, 697 (1997).
[17] I. C. Cloët, W. Bentz, and A. W. Thomas, Phys. Rev. C **90**, 045202 (2014).
[18] A. Freese and I. C. Cloët, Phys. Rev. C **101**, 035203 (2020).
[19] R. T. Cahill, C. D. Roberts, and J. Praschifka, Aust. J. Phys. **42**, 129 (1989).
[20] I. C. Cloët, W. Bentz, and A. W. Thomas, Phys. Lett. B **621**, 246 (2005).
[21] I. C. Cloët, W. Bentz, and A. W. Thomas, Phys. Lett. B **659**, 214 (2008).
[22] H. Mineo, W. Bentz, and K. Yazaki, Phys. Rev. C **60**, 065201 (1999).
[23] I. C. Cloët, W. Bentz, and A. W. Thomas, Phys. Rev. Lett. **95**, 052302 (2005).
[24] G. Eichmann, A. Krassnigg, M. Schwinzerl, and R. Alkofer, Ann. Phys. **323**, 2505 (2008).
[25] D. Nicmorus, G. Eichmann, A. Krassnigg, and R. Alkofer, Phys. Rev. D **80**, 054028 (2009).
[26] H. H. Matevosyan, W. Bentz, I. C. Cloët, and A. W. Thomas, Phys. Rev. D **85**, 014021 (2012).
[27] H. L. L. Roberts, L. Chang, I. C. Cloët, and C. D. Roberts, Few-Body Syst. **51**, 1 (2011).
[28] D. J. Wilson, I. C. Cloët, L. Chang, and C. D. Roberts, Phys. Rev. C **85**, 025205 (2012).
[29] J. Segovia, C. Chen, I. C. Cloët, C. D. Roberts, S. M. Schmidt, and S. Wan, Few-Body Syst. **55**, 1 (2014).
[30] M. E. Carrillo-Serrano, W. Bentz, I. C. Cloët, and A. W. Thomas, Phys. Lett. B **759**, 178 (2016).
[31] G. Eichmann, R. Alkofer, A. Krassnigg, and D. Nicmorus, Phys. Rev. Lett. **104**, 201601 (2010).
[32] G. Eichmann, Phys. Rev. D **84**, 014014 (2011).
[33] T. Horikawa and W. Bentz, Nucl. Phys. A **762**, 102 (2005).
[34] E. R. Berger, F. Cano, M. Diehl, and B. Pire, Phys. Rev. Lett. **87**, 142302 (2001).
[35] V. Yu. Petrov, P. V. Pobylitsa, M. V. Polyakov, I. Bornig, K. Goeke, and C. Weiss, Phys. Rev. D **57**, 4325 (1998).
[36] M. V. Polyakov and C. Weiss, Phys. Rev. D **60**, 114017 (1999).
[37] L. Theussl, S. Noguera, and V. Vento, Eur. Phys. J. A **20**, 483 (2004).
[38] A. V. Vinnikov, arXiv:hep-ph/0604248.
[39] L. X. Gutierrez-Guerrero, A. Bashir, I. C. Cloët, and C. D. Roberts, Phys. Rev. C **81**, 065202 (2010).
[40] S. J. Brodsky, D. S. Hwang, B.-Q. Ma, and I. Schmidt, Nucl. Phys. B **593**, 311 (2001).
[41] I. A. Perevalova, M. V. Polyakov, and P. Schweitzer, Phys. Rev. D **94**, 054024 (2016).
[42] M. Tanabashi *et al.* (Particle Data Group), Phys. Rev. D **98**, 030001 (2018).
[43] C. Alexandrou, M. Constantinou, K. Hadjiyiannakou, K. Jansen, C. Kallidonis, G. Koutsou, A. V. Avilés-Casco, and C. Wiese, Phys. Rev. Lett. **119**, 142002 (2017).
[44] A. W. Thomas, Phys. Rev. Lett. **101**, 102003 (2008).
[45] M. Mazouz *et al.* (Jefferson Lab Hall A Collaboration), Phys. Rev. Lett. **99**, 242501 (2007).
[46] Z. Ye (HERMES Collaboration), Deep inelastic scattering, in *Proceedings of the 14th International Workshop, DIS 2006, Tsukuba, Japan, April 20–24, 2006* (World Scientific, Singapore, 2006), pp. 679–682.
[47] A. Airapetian *et al.* (HERMES Collaboration), J. High Energy Phys. 06 (2008) 066.